Title

Production and Transformation of Mixed-Valent Nanoparticles Generated by Fe(0) Electrocoagulation

Journal

Environmental Science and Technology, 49(4)

ISSN

0013-936X

Authors

Dubrawski, Kristian L
van Genuchten, Case M
Delaire, Caroline
et al.

Publication Date

2015-02-17

DOI

10.1021/es505059d

Peer reviewed

Environmental Science & Technology

Article

pubs.acs.org/est

Production and Transformation of Mixed-Valent Nanoparticles Generated by Fe(0) Electrocoagulation

Kristian L. Dubrawski,[†] Case M. van Genuchten,[‡,⊥] Caroline Delaire,[‡] Susan E. Amrose,[‡] Ashok J. Gadgil,[‡,§] and Madjid Mohseni*,[†]

[†]Department of Chemical and Biological Engineering, University of British Columbia, Vancouver, British Columbia V6T 1Z3, Canada

[‡]Department of Civil and Environmental Engineering, University of California, Berkeley, Berkeley, California 94720-1710, United States

[§]Environmental Energy Technologies Division, Lawrence Berkeley National Laboratory, Berkeley, California 94720, United States

Supporting Information

ABSTRACT: Mixed-valent iron nanoparticles (NP) generated electrochemically by Fe(0) electrocoagulation (EC) show promise for on-demand industrial and drinking water treatment in engineered systems. This work applies multiple characterization techniques (in situ Raman spectroscopy, XRD, SEM, and cryo-TEM) to investigate the formation and persistence of magnetite and green rust (GR) NP phases produced via the Fe(0) EC process. Current density and background electrolyte composition were examined in a controlled anaerobic system to determine the initial Fe phases generated as well as transformation products with aging. Fe phases were characterized in an aerobic EC system with both simple model electrolytes and real groundwater to investigate the formation and aging of Fe phases produced in a system representing treatment of arsenic-contaminated ground waters in South Asia. Two central pathways for magnetite production via Fe(0) EC were identified: (i) as a primary product (formation within seconds when DO absent, no intermediates detected) and (ii) as a transformation product of GR (from minutes to days depending on pH, electrolyte composition, and aging conditions). This study provides a better understanding of the formation conditions of magnetite, GR, and ferric (oxyhydr)oxides in Fe EC, which is essential for process optimization for varying source waters.

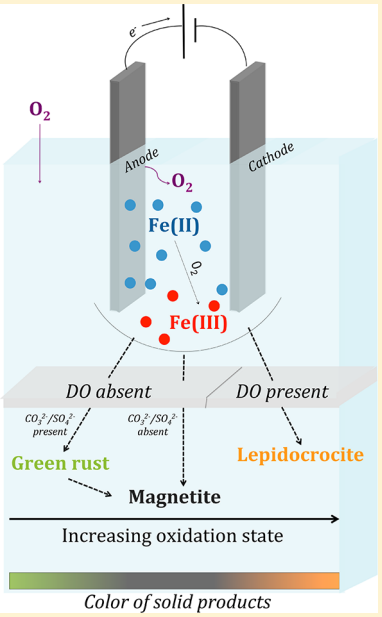

1. INTRODUCTION

Mixed-valent iron (Fe) oxide nanoparticles (NP), such as magnetite and green rust (GR), are commonly used in several environmental applications including as a reducing agent for chromium, nitrate, and uranium,[1−4] for dechlorination of carbon tetrachloride,[5] as a substrate for ion exchange,[6] and, particularly in the case of magnetite, as a magnetically susceptible sorbent for arsenic.[7−10] Conventional synthesis from Fe salts often requires elevated temperature, extended reaction time, and/or precise control of precursor concentrations and solution chemistry,[11] presenting a major challenge for the use of magnetite NP in engineered systems. Furthermore, magnetite NP are known to aggregate in aqueous solution,[12,13] which decreases effectiveness due to reduced reactive surface area,[7] often requiring storage in organic medium, which adds additional costs and may not be feasible in a typical water treatment facility. Electrochemical generation of magnetite, or green rust NP that ultimately transform into magnetite,[14] may offer an alternative for on-demand environmental applications such as the treatment of arsenic-contaminated groundwater, since magnetite NPs could be used as adsorption media for arsenic[9] and subsequently removed from solution by fast magnet-aided settling.[7] Electrochemical generation of magnetite could also allow for onsite production of homogeneous phases without lead times or the use of specialized storage medium.

Whereas the electrochemical formation of Fe oxides, hydroxides, and oxyhydroxides (collectively referred to as iron (oxyhydr)oxides here) under typical passive environmental conditions and time scales (e.g., atmospheric rusting) are well documented,[15,16] the intentional generation of magnetite and GR NP by electrochemical means has been largely overlooked in the context of environmental applications. Rather, most previous work applying Fe-based electrochemical techniques to remediate water supplies has centered on the production of a

Received: October 16, 2014
Revised: January 15, 2015
Accepted: January 21, 2015
Published: January 21, 2015

DOI: 10.1021/es505059d
Environ. Sci. Technol. 2015, 49, 2171−2179

destabilizing charged coagulant in the Fe(0) EC process[17,1819−21] and on characterizing the passive corrosion products of zero-valent iron.[22,23] These studies report end products of ferrimagnetic magnetite,[15,17,22] antiferromagnetic (oxyhydr)oxides (goethite, lepidocrocite, hematite, ferrihydrite),[23−26] ferrimagnetic maghemite,[23,27] and double-layered hydroxide green rusts.[10,24,26] Although the solution conditions for the chemical synthesis of GR and magnetite NP have been well described,[11,15,28,29] the electrochemical pathways are not well documented. To the authors' knowledge, no study has investigated the effect of key solution properties such as electrolyte composition, dissolved oxygen (DO), and pH or electrochemical operating conditions, such as Fe ion flux, current efficiency, and interface potential controlled by current density (i) on the resulting Fe (oxyhydr)oxide phase and morphology. Furthermore, potential mineral transformations of the initially formed precipitate during aging in different chemical environments, which likely govern the long-term reactivity of the EC-generated Fe phase, are also poorly characterized. Additionally, a major technical challenge facing current Fe(0) EC in field operation is in the low-cost separation of colloidally stable nanoscale Fe(III) precipitates from treated water.[30] Incorporating a magnetically susceptible Fe phase with a high specific surface area, such as nanoscale magnetite, into treatment design could eliminate the current need of filtration, coagulation, or settling of nanoscale Fe(III) precipitates.

Understanding the operating parameters, solution chemistry, and aging conditions that drive the formation and transformation of mixed-valent Fe NPs in both deoxygenated and aerobic electrolytes (respectively, representative of freshly pumped and stored groundwater) would grant insight into the fundamental electrode reactions in Fe(0) EC. This knowledge would permit better predictions of the effectiveness of environmental and industrial applications of these Fe phases and could also foster the use of mixed-valent Fe phases in remediation technologies.

To these ends, the objectives in this work are to apply multiple macroscopic, microscopic, and spectroscopic techniques to investigate the formation and persistence of magnetite and GR via Fe(0) EC as a function of current density (i), electrolyte composition, and anaerobic and aerobic aging. We first examine the role of current density and solution chemistry on the formation of mixed-valent Fe mineral phases in a controlled anaerobic system with simple electrolytes. We also identify the operating conditions that lead to the formation of ferric (oxyhydr)oxide phases in the anaerobic system, which are important Fe mineral phases in Fe(0) EC systems due to their persistence as colloidally stable nanoparticles and broadly significant due to the strong affinity of Fe(III) precipitates to bind contaminants.[31] Next, we investigate the formation conditions of mixed-valent Fe phases in an aerobic system beginning with simple model electrolytes and building up to real groundwater. This approach allows us to assess the feasibility of EC-generated magnetite or GR for treatment of aerobic natural waters with particular emphasis on arsenic removal (i.e., groundwater pumped or stored with exposure to atmospheric oxygen). Lastly, we identify the intermediate Fe (oxyhydr)oxide phases and their transformation products while aging in aerobic and anaerobic conditions and discuss the implications of these phase transformations on the application of EC to generate magnetite as a ferromagnetic sorbent in engineered systems.

2. MATERIALS AND METHODS

2.1. Anaerobic Cell Experiments. We constructed two different anaerobic electrochemical cells under N_2 atmosphere to act as highly controlled EC reactors. The first cell was used for Fe concentration measurements and consisted of a 50 mL acrylic cell, a 99.9% pure Fe(0) anode (Goodfellow Cambridge Ltd.) of 100 mm^2 area and 1 mm thickness, and a 99.99% pure Pt(0) (Goodfellow Cambridge Ltd.) cathode of 100 mm^2 and 0.2 mm thickness with an interelectrode gap of 50 mm. A second microcell was identical in design but scaled down to 0.5 mL using 1 mm^2 electrodes with an interelectrode gap of 0.5 mm. This cell contained N_2 ports to prevent oxidation by atmospheric O_2 during analysis and was designed to accommodate precipitate characterization by in situ Raman spectroscopy and cryogenic transmission electron microscopy (cryo-TEM) (Figure S1, Supporting Information). Electrodes for both anaerobic cells were connected via glass-insulated copper wire to a galvanostatic dc current source (Princeton Applied Research, Versastat 3). Before each experiment, electrodes were wet polished with alumina paste, rinsed with 1% sulfuric acid, and double rinsed with 18 MΩ ultrapure water (Millipore Milli-Q). The impact of three parameters (i, solute type, and solute concentration) on the reactions occurring at the anode and the resulting Fe (oxyhydr)oxide phase were investigated. We examined i values ranging from 5 to 125 mA/cm^2, corresponding to a range of charge loading rates (CLR) (6−150 C/L/min) that have been reported to lead to different Fe phases.[32] Charge loading (CL) was maintained constant (30 C/L) for each i value by keeping electrode areas constant, changing the applied current, and adjusting electrolysis time accordingly. Theoretical Fe dissolution (Fe_t) was calculated using Faraday's law of electrolysis, based on eq 1

$$[Fe_t] = CL^*M_{Fe}/(F\cdot z) \quad (1)$$

where M_{Fe} is the molar mass of iron (55.845 g/mol), F is Faraday's constant (96 485 C/mol), and z is the charge transfer coefficient, with $z = 2$ for Fe (as reported elsewhere for similar EC experiments[20,32]).

The electrolytes used in the anaerobic cell were composed of ultrapure water amended with different concentrations of Na_2SO_4 (3 and 9 mM) and/or NaCl (0, 0.3, 1, and 3 mM) (Laboratory grade, Fisher Scientific) and deoxygenated prior to use by purging $N_{2(g)}$ for 6 h. The initial pH was adjusted to 7.0 ± 0.1 by adding 0.01 M NaOH or H_2SO_4 (Laboratory grade, Fisher Scientific). Experimental Fe concentrations ($[Fe_e]$) were measured by inductively coupled plasma optical emission spectroscopy (ICP-OES) with wavelengths of 238.204 and 239.562 nm (PerkinElmer Optima 7300 DV). Bulk DO was monitored (YSI 50B)—we note that although bulk DO did not change significantly, localized DO changes near the electrode surface reactions might have occurred but were not measurable.

2.2. Aerobic Cell Experiments. The aerobic cell was fabricated to be a more realistic cell design for Fe EC as it might be used in a rural community water treatment center and consisted of two parallel iron electrodes (McMaster Carr, mild steel) with a surface area of 1000 mm^2 and an interelectrode gap of 10 mm. Experiments were conducted in 200 mL of electrolyte at i = 5, 10, and 20 mA/cm^2, corresponding to CLR values ranging from 15 to 60 C/L/min. Current densities were smaller in the aerobic cell than in the anaerobic cell to provide a more realistic indication of EC formation products at practical power constraint limits in natural waters. We used unbuffered

DOI: 10.1021/es505059d
Environ. Sci. Technol. 2015, 49, 2171−2179

(5 mM NaCl, 2.5 mM $CaCl_2$, and 2.5 mM $MgCl_2$) and buffered solutions containing 10 mM $NaHCO_3$ (with and without 0.04 mM Na_2HPO_4) as a range of simple synthetic electrolytes with similarities to groundwaters of interest. We also used real groundwater collected from West Bengal, India (6 mM alkalinity, 0.6 mM Si, 7 μM P, 2.5 mM Ca^{2+}, 1.6 mM Mg^{2+}, negligible Fe) to investigate Fe (oxyhydr)oxide formation in an electrolyte similar to arsenic-contaminated aquifers in South Asia. Arsenic concentration was low (<20 μg/L) in the real groundwater, and removal was not measured, since we were primarily concerned with the structure of the precipitate, which was not expected to be affected by low levels of As compared to the higher concentrations of HCO_3, Si, and P. Likewise, minor components were not measured in the real groundwater (e.g., Mn, S, dissolved organic carbon) but were not expected to significantly impact the formation of Fe precipitates. Experiments began at saturated DO and neutral pH, except where specified otherwise. Charge loadings of 600−3600 C/L were chosen for both synthetic and real groundwaters in the aerobic cell to simulate typical loadings required to decrease arsenic below the WHO drinking water guidelines of 10 ppb in EC field treatment.[30,33] For the aerobic cell, EC precipitates were allowed to settle and age either open to the atmosphere or in an anaerobic chamber (simulating both closed and open atmospheric storage of EC-treated waters in typical rural community settings) for 1−14 days. Aging times were selected to ensure transformations were observed and 4 days and 1 day for aerobic and anaerobic aging, respectively, and 2 weeks and 4 days, respectively, for the real groundwater sample.

2.3. Solid-Phase Characterization. For the anaerobic microcell, EC precipitates were characterized using a Raman spectroscopy system (InVia, Renishaw) equipped with a 785 nm, 160 mW (at 1% = 1.6 mW) excitation laser and 40× wet objective (Leica HCX APO 40×). The Raman wet-objective probe was immersed in the microcell solution focused in the plane between the electrodes with a 12.7 mm diameter Au mirror (Thorlabs Inc.) fixed underneath (Figure S1, Supporting Information). It should be noted that the low laser strengths used in our study are not likely to induce mineral phase transformations, as seen elsewhere for a similar range of laser strengths.[34] Samples from both anaerobic cells were also analyzed using SEM (Hitachi S-2300) and a cryogenic-equipped TEM (FEI Tecnai G2 200 kV LaB_6). For the anaerobic cell, phase and crystallinity of the precipitates generated were characterized by X-ray diffraction (XPERT-PRO diffractometer). In situ Raman and cryo-TEM were not compatible with the larger volume of the aerobic cell. Samples prone to oxidation (i.e., green rust) were mixed with a drop of glycerol immediately after filtration to avoid oxidation during XRD analysis, following Hansen.[35] Further details of in situ Raman, SEM, cryo-TEM, and XRD techniques can be found in Text S1 (Supporting Information).

3. RESULTS AND DISCUSSION

3.1. Impact of *i* on Fe (Oxyhydr)oxide Formation in the Anaerobic Cell. We first investigated the impact of i on the formation of magnetite in the anaerobic cell by examining the role of this parameter on the electron transfer reactions occurring at the Fe(0) anode. In this work we define the Faradaic current efficiency, φ, as the ratio of experimentally measured Fe concentration ($[Fe_e]$) over ($[Fe_t]$) as calculated by eq 1. By comparing the φ value of each sample, we are able to estimate the relative contributions of different anodic reactions that can proceed at a given i. Consistent with the work of Lakshmanan et al. 2010, we assume that the two dominant anodic reactions are the production of Fe(II) and O_2[20]

$$Fe \rightleftharpoons Fe(II) + 2e^- \quad (2)$$

$$H_2O \rightleftharpoons 1/2O_2 + 2H^+ + 2e^- \quad (3)$$

Table 1 shows the φ values for i ranging from 5 to 125 mA/cm^2 (3 mM Na_2SO_4 + 0 mM NaCl). At i = 5 mA/cm^2, φ was 0.93, suggesting that reaction 2 was the primary reaction occurring at the anode. At i = 125 mA/cm^2, φ was found to be 0.15, suggesting that the majority of the applied current generated O_2 by reaction 3. The drop in φ due to the anodic production of O_2 is consistent with our observation of bubbles on the anode at this i value, which was also observed at similar i in previous work.[36] The absence of Cl^- in the electrolyte rules out the anodic production of $Cl_{2(g)}$. Predictably, i = 25 mA/cm^2 gave an intermediate φ = 0.43, suggesting that both reactions 2 and 3 occurred.

Table 1. Impact of *i* and Electrolyte Composition on Current Efficiency, Reaction Products, and Intermediate GR Formation in the Anaerobic Cell[a]

electrolyte	current density (mA/cm^2)	Faradic efficiency	end product of EC	intermediate GR
Na_2SO_4 (3 mM)	5	0.93	Mag	yes[b]
	10	0.74	Mag + Lp	no
	25	0.43	Lp	no
	125	0.15	Lp	no
Na_2SO_4 (3 mM) + NaCl (0.3 mM)	5	0.96	Mag	yes[b]
	25	0.93	Mag	yes
	125	0.62	Lp	no
Na_2SO_4 (3 mM) + NaCl (1 mM)	5	0.93	Mag	yes[b]
	25	0.85	Mag	yes
	125	0.84	Mag	yes
Na_2SO_4 (9 mM) + NaCl (3 mM)	125	0.53	Lp	no

[a]Reaction products were characterized by in situ Raman. Mag = magnetite; Lp = lepidocrocite; GR = green rust. [b]GR was observed visually but not with in situ Raman.

At low φ in the anaerobic cell we expect that the O_2 produced at the anode goes on to rapidly oxidize Fe(II), also produced at the anode, resulting in primarily ferric (oxyhydr)-oxide precipitates. Indeed, cryo-TEM images showed 100−200 nm aggregates of 10−30 nm needle-like particles formed during the experiments carried out at i = 125 mA/cm^2 (Figure 1), which is consistent with the morphology of lepidocrocite.[37] While it is difficult to differentiate mineral phase based exclusively on morphology, lepidocrocite is a well-known product of Fe(II) oxidation by DO in background electrolytes like NaCl, $NaHCO_3$, or Na_2SO_4.[38,39] Nanocrystalline hydrous ferric oxide, which was observed in previous EC studies,[25] is not likely to form in these samples due to the absence of strongly adsorbing ions. Conversely, cryo-TEM images of the precipitates generated at i = 5 mA/cm^2, where significant O_2 evolution is unlikely, showed a different morphology consisting of 25−85 nm cubic particles, which is consistent with magnetite crystal morphology.[40]

In the anaerobic EC cell, we assume that O_2 evolution is negligible at i = 5 mA/cm^2 based on the measured φ value near

DOI: 10.1021/es505059d
Environ. Sci. Technol. 2015, 49, 2171−2179

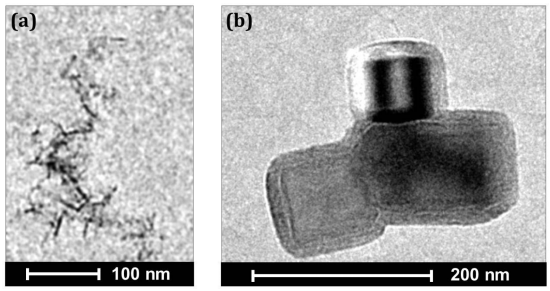

Figure 1. Cryo-TEM images showing the impact of i on Fe(0) EC formation products for [Na_2SO_4] = 3 mM, [NaCl] = 0 mM; (a) i = 125 mA/cm^2 showing aggregates of 10−20 nm needles; (b) i = 5 mA/cm^2 showing 50−100 nm octahedral magnetite.

unity. If no DO is present in solution, the observed formation of magnetite requires some Fe(III) to be produced through an anaerobic reaction. A recent study reported the formation of Fe(III)-containing magnetite and green rust from polarized steel in an anaerobic cell, but the source of Fe(III) was not identified.[41] Although it is not possible to identify the origin of Fe(III) in the i = 5 mA/cm^2 sample with our data set, possible anaerobic reactions might include the Schikorr reaction[42] or direct anodic oxidation of Fe(II) to Fe(III).

A clear trend of decreasing φ with increasing i appears in the anaerobic cell experiments, contrary to previous work that showed Fe(II) generation was independent from i within the range of i tested here.[20] The observed trend is best explained by the relationship of i and anode interface potential governed by the Butler−Volmer relationship, eq 4

$$i = i_0 \cdot \left\{ \exp\left[\frac{\alpha_a z F \eta}{RT}\right] - \exp\left[\frac{\alpha_c z F \eta}{RT}\right] \right\} \quad (4)$$

where i_0 is the exchange current density, η is the overpotential, R is the universal gas constant, T is the absolute temperature, and α_a and α_c are the anodic and cathodic charge transfer coefficients, respectively. As current density increases from i = 5 to 125 mA/cm^2, a decrease in φ is the result of two interdependent phenomena: (i) the anodic interface potential (governed by η) increases with increasing i by eq 2 to a value at which the primary electron transfer reaction favored at the anode surface is the evolution of O_2 by reaction 3, and (ii) the greater anodic surface potential at higher i likely increased the thickness of the passivation layer with the presence of passivation promoting ions (e.g., SO_4^{2-}), as seen with aluminum electrodes in EC.[43] This would facilitate O_2 evolution at higher i, as seen in our previous work.[44]

3.2. Impact of Electrolyte Composition on Fe (Oxyhydr)oxide Formation in the Anaerobic Cell. In the anaerobic cell, for a given i the composition of the electrolyte had a notable impact on the φ value and thus formation of magnetite. The addition of 0.3 mM NaCl led to an increase from φ = 0.43 to φ = 0.93 at 25 mA/cm^2 and from φ = 0.15 to φ = 0.62 at 125 mA/cm^2. An increase to 1.0 mM NaCl further increased Fe(0) dissolution for all i values (Table 1). Magnetite was observed as the primary solid phase produced at φ > 0.75 (e.g., i = 25 mA/cm^2, 0.3 mM NaCl or i = 125 mA/cm^2, 1 mM NaCl), whereas Fe(III) (oxyhydr)oxides dominated otherwise.

Although the increase in electrolyte conductivity upon addition of NaCl could contribute to a reduction in interface potential, and thus decrease the likelihood of O_2 evolution, this was not likely due to the lack of increased φ at higher [Na_2SO_4] and greater conductivity. Rather, the increase in φ in the presence of NaCl, and thus formation of magnetite in lieu of Fe(III) precipitates, could be explained by the role of Cl^- altering the surface properties of the Fe(0) anode. Chloride ions are well known to promote localized pitting and crevice corrosion, which increases the anodic surface area by creating microscopic abrasions on EC electrodes.[43] In this case, the effective surface area of the Fe(0) electrode would be larger than previously measured, thus decreasing the effective current density, and by eq 4, the anodic potential and likelihood for O_2 production would also decrease. Furthermore, Cl^- is also recognized to dissolve or inhibit the formation of Fe (oxyhydr)oxide passive layers on Fe(0),[45] which would lead to a decrease in anodic interface potential, favoring a larger φ.

When [Na_2SO_4] and [NaCl] were increased 3-fold to 9 and 3 mM, respectively (keeping the [SO_4^{2-}]:[Cl^-] ratio constant), φ decreased from 0.84 to 0.53 at i = 125 mA/cm^2, suggesting that a higher [SO_4^{2-}] inhibited the effects of increased [Cl^-], which is consistent with previous work using aluminum electrodes.[46] The decreased φ value observed with increased solution conductivity suggests that the concentration of passivation promoting SO_4^{2-} had a greater impact than decreased iR resistivity on O_2 evolution. Only Fe(III)

Table 2. Impact of i, Electrolyte Composition, and Aging Conditions on the Reaction Products and Intermediate GR Formation in the Aerobic Cell[a]

electrolyte	pH (initial:final)	current density (mA/cm^2)	final DO (% of saturation)	end product of EC	product of anaerobic aging	product of aerobic aging
NaCl (5 mM)	7.5:10	5	30%	Lp*		
		10	<5%	Mag		Mag
		20	<5%	Mag*		Mag
$CaCl_2$ (2.5 mM)	7.5:10	20	<5%	Mag		
$MgCl_2$ (2.5 mM)	7.5:8.1	20	<5%	Mag		
NaCl (5 mM)	7:7.5	20	<5%	GR(CO_3^{2-})*	Mag*	Mag + Goet + Lp*
+ $NaHCO_3$ (10 mM)	9.5:10	20	<5%	Mag*		Mag
NaCL (5 mM) + $NaHCO_3$ (10 mM) + Na_2HPO_4 (0.1 mM)	9.5:10	20	<5%	GR(CO_3^{2-})*	Mag*	Mag + Goet + Lp*
groundwater	7.5:8	20	<5%	GR(CO_3^{2-})	Mag*	Mag + Goet*

[a]Aerobic and anaerobic aging times were 4 days and 1 day, respectively (2 weeks and 4 days, respectively, for the real groundwater sample). Aging products were characterized by XRD. Mag = magnetite; Lp = lepidocrocite; Goet = goethite; GR = green rust. Asterisks (*) indicate samples for which XRD data are given in Figure 2.

DOI: 10.1021/es505059d
Environ. Sci. Technol. 2015, 49, 2171−2179

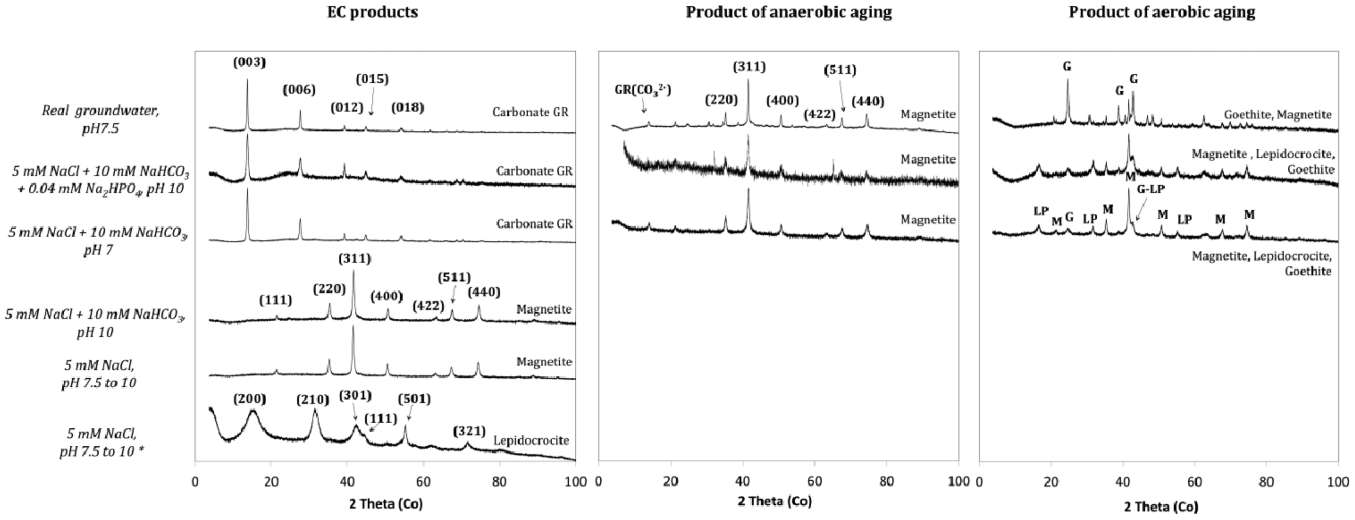

Figure 2. XRD characterization of EC products in the aerobic cell. All samples were obtained at i = 20 mA/cm^2, except the sample marked with an asterisk (*) obtained at i = 5 mA/cm^2. Miller indices are indicated for carbonate GR and magnetite. Characteristic peaks for magnetite and Fe(III) (oxyhydr)oxides are indicated on the right side of each spectra. Aerobic and anaerobic aging times were 4 days and 1 day, respectively (2 weeks and 4 days, respectively, for the real groundwater sample).

(oxyhydr)oxide precipitates were observed in this sample presumably due to O_2 evolution, which suggests that magnetite generation may prove difficult in anaerobic EC cells operated at high current density in electrolytes containing high [SO_4^{2-}] even in the presence of a high concentration of Cl^-.

3.3. Impact of *i* and Electrolyte Composition on Fe (Oxyhydr)oxide Formation in the Aerobic Cell. Table 2 summarizes the resulting Fe phase and DO concentrations obtained in the aerobic EC cell for different i values ranging from 5 to 20 mA/cm^2 in different electrolytes. At i = 5 mA/cm^2 in 5 mM NaCl, a significant value of DO (30%) was measured and only lepidocrocite was detected in the solid phase (Figure 2). However, higher i values (10 and 20 mA/cm^2) in the same electrolyte led to low final DO (<5%), and the formation of magnetite rather than Fe(III) precipitates was observed. The formation of magnetite was also observed in electrolytes consisting of 2.5 mM $CaCl_2$ or $MgCl_2$ at i = 20 mA/cm^2 (final DO < 5%), suggesting a minimal impact of Ca^{2+} or Mg^{2+} on the mineral phase. Conversely, when EC was applied to the aerobic cell in a circumneutral bicarbonate electrolyte (5 mM NaCl + 10 mM $NaHCO_3$, buffered at pH 7−7.5), we observed the initial formation of carbonate GR based on the known basal plane (d_{003}) d-spacing value of 7.5 Å.[47] X-ray diffraction confirmed the formation of carbonate GR in real groundwater at i = 20 mA/cm^2 as well, suggesting that the formation of carbonate GR is favored in most natural systems where $NaHCO_3$ is present (in situ Raman spectra in the microcell were not able to differentiate between types of GR). However, in contrast to the high stability observed in EC-generated magnetite, the GR phase formed in electrolytes containing $NaHCO_3$ was unstable and transformed to a variety of different mineral phases depending on aging conditions, which is discussed in the following section.

For all i values (5−20 mA/cm^2) in the aerobic cell, φ was close to unity and we considered anodic O_2 evolution insignificant. The decrease in residual DO and thus formation of mixed-valent Fe phases with increasing i in the aerobic cell can be explained by the greater Fe(II) production rate at higher i, which leads to faster consumption of DO than can be replenished by atmospheric O_2 influx. Consistent with the anaerobic cell results, magnetite only formed when the final DO was very low (<5%), whereas lepidocrocite was produced when DO was present in greater concentrations. These results suggest that the DO concentration is a key parameter driving the formation of mixed-valent Fe phases in both the anaerobic and the aerobic cells. At low i values, the relationship between i and the production of mixed-valent Fe phases in the aerobic cell is the opposite of this relationship in the anaerobic cell. At low i in the aerobic cell, significant DO remained throughout electrolysis and only Fe(III) (oxyhydr)oxides were produced, whereas at low i in the anaerobic cell, O_2 generation was minimal and magnetite formed. However, we expect that if i increases in the aerobic cell above the value at which anodic O_2 production is the dominant electrode reaction (e.g., 125 mA/cm^2 in the anaerobic cell), the same relationship between i and magnetite will eventually hold for both anaerobic and aerobic cells.

The results for the aerobic cell show promise for engineered systems due to the predominantly magnetite end product at intermediate i in simplified electrolytes (e.g., Na^+, Cl^-, Ca^{2+}, Mg^{2+}). However, the predominant generation of a GR in the presence of bicarbonate suggests that immediate separation of As-loaded magnetite by a low-strength magnetic field is not likely in most waters. Rather, the production of EC-generated magnetite in aerobic systems with natural groundwater will likely rely on phase transformations and aging products.

3.4. Phase Transformation of Fe (Oxyhydr)oxide Intermediates in the Anaerobic and Aerobic Systems. In the anaerobic cell at any i (5−125 mA/cm^2) with chloride present in higher concentrations ([Na_2SO_4] = 3 mM, [NaCl] = 1 mM), a green rust (GR) intermediate that eventually transformed into magnetite was observed by in situ Raman, SEM, and cryo-TEM. SEM images shown in Figure S2 (Supporting Information) reveal hexagonal plates of approximately 150 nm in size, consistent with the hexagonal morphology of GR.[48] In the cases where GR was detected in the anaerobic cell, it was observed only transiently, transforming within minutes to either lepidocrocite or magnetite depending on aging conditions. At higher φ (>0.8) with insignificant oxygen evolution, GR transformed to magnetite.

DOI: 10.1021/es505059d
Environ. Sci. Technol. 2015, 49, 2171−2179

Consistent with this transformation, the TEM images in Figure 3A show 150 nm hexagonal GR crystallites and 400 nm

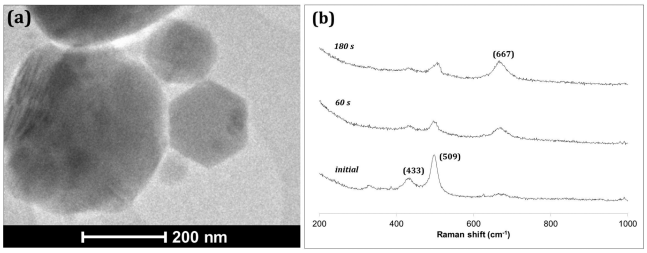

Figure 3. (a) In situ cryo-TEM showing simultaneous GR and magnetite occurrence, possibly during transformation of GR to magnetite; (b) in situ Raman spectra for GR transformation to magnetite in 180 s; reference peaks for GR at 432 and 509 cm^{-1} [34] and magnetite at 667 cm^{-1} [49] are indicated.

magnetite particles occurring simultaneously. Providing further evidence for the transformation of GR to magnetite in the anaerobic cell, the Raman spectra of the same sample show a gradual increase in the peak at 667 cm^{-1} for magnetite at the expense of the GR peaks at 433 and 509 cm^{-1}, where peaks for magnetite and GR follow previous research[34,49] (Figure 3B). Samples analyzed after several hours showed no evident Raman or XRD peaks for GR. Since GR transforms through a dissolution−precipitation process,[50] the fast transformation kinetics seen here may be attributed to the alkaline pH, which promotes oxides dissolution.[51] At higher *i* (125 mA/cm^2) in low chloride concentrations ($[Na_2SO_4]$ = 3 mM, [NaCl] = 0 or 0.3 mM), the only solid-phase products observed were Fe(III) (oxyhydr)oxides due to O_2 evolution. Using Raman spectroscopy, we observed the well-documented mineral transformation from primarily lepidocrocite to primarily goethite[11] when aged for 7 days (Figure S3, Supporting Information). However, we do not expect a pure goethite product to form over this time scale due to the slow kinetics of this mineral transformation. Indeed, minor residual Raman peaks at 252, 380, and 654 cm^{-1} were observed in aged sample.

In the aerobic cell at high *i*, magnetite formed in all electrolytes (either as an end product of EC or after aging) except for those containing $NaHCO_3$. This magnetite phase did not undergo phase transformation in aerobic aging conditions in NaCl, suggesting that magnetite formed in the EC process is stable—the stability of magnetite produced during aqueous corrosion has been observed by others.[11,28] However, consistent with the results in the anaerobic cell, the GR phase formed in the presence of $NaHCO_3$ transformed rapidly depending on aging conditions. When aged in an anaerobic chamber, the GR phase transformed into pure magnetite within 24 h. Conversely, when aged open to the atmosphere, GR transformed into a mixture of magnetite, goethite, and lepidocrocite (Table 2 and Figure 2), which is consistent with previously reported anaerobic and aerobic transformations of GR.[50] Interestingly, when the same bicarbonate buffered electrolyte was maintained at pH 9.5 in the aerobic cell, the final product was pure magnetite, with a much shorter lived (several minutes) intermediate GR phase. This result points to the accelerated dissolution−precipitation of GR at alkaline pH values as discussed earlier, allowing GR transformation before DO is replenished from atmosphere.

Phosphate, a common groundwater ion that often influences mineral phases in natural systems, was examined for its impact on the transformation of the transient GR in the aerobic cell by adding 0.04 mM Na_2HPO_4 to the 5 mM NaCl + 10 mM $NaHCO_3$ electrolyte buffered at pH 9.5. We observed a similar carbonate GR intermediate product; however, the transformation of the GR phase to relatively pure magnetite in anaerobic conditions required 24 h instead of minutes. The slower transformation kinetics in the presence of phosphate is likely due to adsorbed phosphate ions inhibiting GR dissolution by acting as a physical barrier against the release of interlayer CO_3^{2-} ions, as seen with the effect of phosphate on the transformation of carbonate green rust elsewhere.[52] Our results thus suggest that GR evolution to magnetite can be retarded in the presence of strongly adsorbed oxyanions that are common in natural systems.

In natural groundwater from West Bengal, India, GR transformation to magnetite was only observed after 4 days when aged anaerobically, which is significantly longer than in previous experiments with simplified electrolytes. As we have shown, alkaline pH values and the absence of strongly sorbing oxyanions (e.g., phosphate) leads to increased rates of GR transformation to magnetite. The real groundwater used in our study contained high concentrations of phosphate and silicate at a circumneutral pH. Predictably, GR transformation to

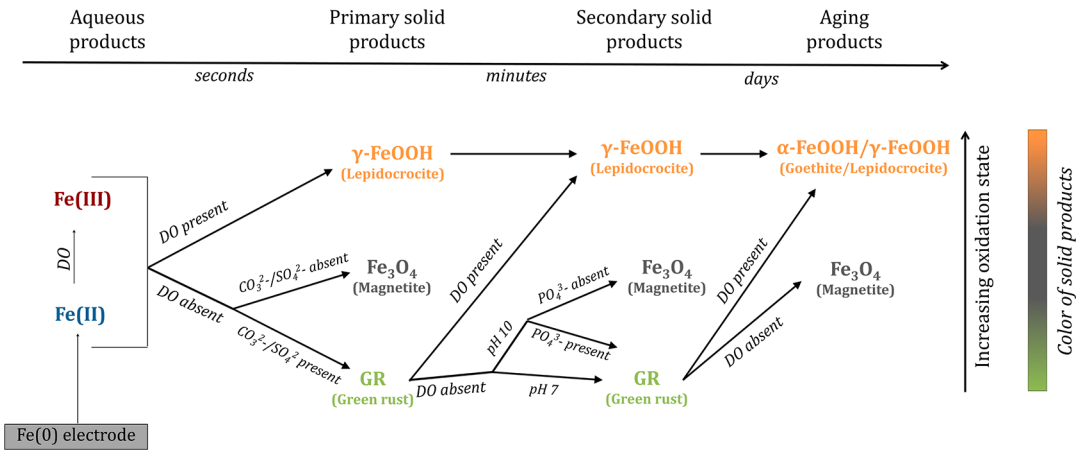

Figure 4. Schematic diagram of the formation pathways of mixed-valent Fe hydr(oxide) phases generated by Fe(0) electrocoagulation. As Fe(II) is oxidized to Fe(III) by DO (either existing in the aerobic cell or via oxidation of water in the anaerobic cell), mixed-valent species are formed.

DOI: 10.1021/es505059d
Environ. Sci. Technol. 2015, 49, 2171−2179

magnetite in real groundwater was markedly slower than in our experimental synthetic electrolytes in the aerobic cell, likely due to strongly sorbing Si and P oxyanions. When the GR that formed in real groundwater was aged in the open air for 2 weeks, the end products were a mixture of magnetite and goethite (Table 2). Exposure to atmospheric O_2 likely led to more rapid oxidation of GR and to the formation of goethite, which is consistent with previous work.[50] However, atmospheric O_2 was likely consumed by GR near the liquid surface, leading to GR transformation to magnetite at greater depths where there was no exposure to O_2. These results suggest that groundwater remediation based on EC-generated magnetite would thus require anaerobic aging of primary EC products if the adsorbent were generated in situ. One simple and potentially appropriate method for creating such an anaerobic environment in rural settings to permit magnetite production from GR transformation is as follows: run the EC cell at high *i* to ensure that EC-generated Fe(II) consumes DO faster than can be replenished by atmospheric oxygen influx, followed by sealing the deoxygenated volume, and allow for the aging and transformation of GR to proceed. This two-step method, which would incorporate a low-strength magnetic field to separate magnetite particles, could eliminate the need for filtration or settling of colloidally stable nanoscale Fe(III) precipitates typically observed in Fe(0) EC systems.

3.5. Pathways of Magnetite Formation and Implications for Environmental Remediation Using EC-Generated Mixed-Valent Fe (Oxyhydr)oxides. The different conditions for magnetite and GR formation observed in this study are summarized in Figure 4. Overall, mixed-valent Fe phases only formed when DO was absent or very low. Two main pathways for magnetite production via Fe(0) EC were identified: (i) as a primary product (formation within seconds; no intermediates detected with our techniques) and (ii) as a transformation product of GR (from minutes to days depending on pH, electrolyte composition, and aging conditions). In cases where GR formed as a precursor for magnetite in the aerobic cell, the transformation into magnetite was considerably slower, likely due to oxyanions adsorbed to GR surfaces. This reduction in transformation kinetics could complicate the synthesis of high-purity magnetite by Fe(0) EC in natural waters due to the extended aging time required for magnetite formation in anaerobic containers. However, the slow transformation of GR to magnetite observed in the natural groundwater sample might also improve the efficacy of contaminant removal; the longer persistence of the GR phase can result in additional time for pollutant (e.g., arsenic) sorption to GR before transformation to magnetite. As shown in our SEM images, EC-generated GR is characterized by a much smaller crystallite size than the magnetite into which it transforms, which presumably leads to a significant loss of specific surface area upon transformation. The fate of sorbed contaminants during the transformation from EC-generated GR to magnetite could consequently involve a concomitant release of surface-bound contaminants. However, recent studies have shown that some contaminants, such as arsenic, can substitute for tetrahedral Fe and become incorporated in the spinel-type magnetite (and maghemite) structures, which is then expected to significantly enhance contaminant uptake stability.[53,54] Accordingly, the fate of contaminants, particularly arsenic, during the transformation of GR to magnetite is not straightforward and requires additional work to accurately determine the feasibility of EC-generated magnetite or GR as a practical option for environmental remediation. Magnetite formation in arsenic-contaminated groundwater will be complicated by the presence of an intermediary GR(CO_3^{2-}) phase and the need for anaerobic aging. More work is ongoing to quantify arsenic removal before, during, and after GR(CO_3^{2-}) transformation to magnetite.

■ ASSOCIATED CONTENT

Supporting Information

Details on analytical procedures; Microcell configuration used for in situ Raman spectroscopy and cryo-TEM; SEM image of GR, with orthogonal hexagonal crystal plates highlighted; in situ Raman transformation spectra for lepidocrocite transformation to goethite. This material is available free of charge via the Internet at http://pubs.acs.org.

■ AUTHOR INFORMATION

Corresponding Author

*Phone: 604-822-0047. E-mail: Madjid.mohseni@ubc.ca.

Present Address

⊥Institute of Earth Surface Dynamics, University of Lausanne, Lausanne 015-CH, Switzerland

Funding

This study was financially supported by the Natural Science and Engineering Research Council of Canada, the A. J. and Catherine Orselli Fund, the Robert B. Rothschild, Jr. Memorial Fellowship, the Trussell Fellowship in Environmental Engineering, and the Maybelle B. Tucker and John T. Tucker Fund. The authors acknowledge Michael Smith Laboratories and Bio-Imaging Facility (UBC) and also Tim Teague and Haizhou Liu (UC Berkeley).

Notes

The authors declare no competing financial interest.

■ REFERENCES

(1) Hu, J.; Lo, I. M. C.; Chen, G. Removal of Cr(VI) by magnetite nanoparticle. *Water Sci. Technol.* **2004**, *50*, 139−146.

(2) Latta, D. E.; Gorski, C. A.; Boyanov, M. I.; O'Loughlin, E. J.; Kemner, K. M.; Scherer, M. M. Influence of magnetite stoichiometry on U(VI) reduction. *Environ. Sci. Technol.* **2012**, *46*, 778−786.

(3) Williams, A. G. B.; Scherer, M. M. Kinetics of Cr(VI) Reduction by Carbonate Green Rust. *Environ. Sci. Technol.* **2001**, *35*, 3488−3494.

(4) Hansen, H. C. B.; Koch, C. B.; Nancke-Krogh, H.; Borggaard, O. K.; Sørensen, J. Abiotic Nitrate Reduction to Ammonium: Key Role of Green Rust. *Environ. Sci. Technol.* **1996**, *30*, 2053−2056.

(5) Vikesland, P. J.; Heathcock, A. M.; Rebodos, R. L.; Makus, K. E. Particle Size and Aggregation Effects on Magnetite Reactivity toward Carbon Tetrachloride. *Environ. Sci. Technol.* **2007**, *41*, 5277−5283.

(6) Nixon, L.; Koval, C. A.; Noble, R. D.; Slaff, G. S. Preparation and characterization of novel magnetite-coated ion-exchange particles. *Chem. Mater.* **1992**, *4*, 117−121.

(7) Yavuz, C. T.; Mayo, J. T.; Yu, W. W.; Prakash, A.; Falkner, J. C.; Yean, S.; Cong, L.; Shipley, H. J.; Kan, A.; Tomson, M.; et al. Low-field magnetic separation of monodisperse Fe_3O_4 nanocrystals. *Science* **2006**, *314*, 964−967.

(8) Shipley, H. J.; Yean, S.; Kan, A. T.; Tomson, M. B. Adsorption of arsenic to magnetite nanoparticles: effect of particle concentration, pH, ionic strength, and temperature. *Environ. Toxicol. Chem.* **2009**, *28*, 509−515.

(9) Dixit, S.; Hering, J. G. Comparison of Arsenic(V) and Arsenic(III) Sorption onto Iron Oxide Minerals: Implications for Arsenic Mobility. *Environ. Sci. Technol.* **2003**, *37*, 4182−4189.

(10) Su, C.; Puls, R. W. Significance of Iron(II,III) Hydroxycarbonate Green Rust in Arsenic Remediation Using Zerovalent Iron in Laboratory Column Tests. *Environ. Sci. Technol.* **2004**, *38*, 5224−5231.

DOI: 10.1021/es505059d
Environ. Sci. Technol. 2015, 49, 2171−2179

(11) Cornell, R. M.; Schwertmann, U. *The Iron Oxides: Structure, Properties, Reactions, Occurrences and Uses*; Wiley-VCH: New York, 2003; p 703.
(12) Sahoo, Y.; Goodarzi, A.; Swihart, M. T.; Ohulchanskyy, T. Y.; Kaur, N.; Furlani, E. P.; Prasad, P. N. Aqueous ferrofluid of magnetite nanoparticles: Fluorescence labeling and magnetophoretic control. *J. Phys. Chem. B* **2005**, *109*, 3879−3885.
(13) Chanana, M.; Jahn, S.; Georgieva, R.; Lutz, J.-F.; Bäumler, H.; Wang, D. Fabrication of Colloidal Stable, Thermosensitive, and Biocompatible Magnetite Nanoparticles and Study of Their Reversible Agglomeration in Aqueous Milieu. *Chem. Mater.* **2009**, *21*, 1906−1914.
(14) Tamaura, Y.; Yoshida, T.; Katsura, T. The synthesis of green rust II($FeIII_1$-$FeII_2$) and its spontaneous transformation into Fe3O4. *Bull. Chem. Soc. Jpn.* **1984**, *57*, 2411−2416.
(15) Odziemkowski, M. S.; Schuhmacher, T. T.; Gillham, R. W.; Reardon, E. J. Mechanism of oxide film formation on iron in simulating groundwater solutions: Raman spectroscopic studies. *Corros. Sci.* **1998**, *40*, 371−389.
(16) Revie, R. W. *Corrosion and Corrosion Control*; Wiley-Interscience: New York, 2008; p 512.
(17) Tsouris, C.; DePaoli, D. .; Shor, J. .; Hu, M. Z.-C.; Ying, T.-Y. Electrocoagulation for magnetic seeding of colloidal particles. *Colloids Surf., A: Physicochem. Eng. Asp.* **2000**, *177*, 223−233.
(18) Parga, J. R.; Cocke, D. L.; Valenzuela, J. L.; Gomes, J. A.; Kesmez, M.; Irwin, G.; Moreno, H.; Weir, M. Arsenic removal via electrocoagulation from heavy metal contaminated groundwater in La Comarca Lagunera México. *J. Hazard. Mater.* **2005**, *124*, 247−254.
(19) Bagga, A.; Chellam, S.; Clifford, D. A. Evaluation of iron chemical coagulation and electrocoagulation pretreatment for surface water microfiltration. *J. Membr. Sci.* **2008**, *309*, 82−93.
(20) Lakshmanan, D.; Clifford, D. A.; Samanta, G. Ferrous and Ferric Ion Generation During Iron Electrocoagulation. *Environ. Sci. Technol.* **2009**, *43*, 3853−3859.
(21) Cañizares, P.; Jiménez, C.; Martínez, F.; Sáez, C.; Rodrigo, M. A. Study of the Electrocoagulation Process Using Aluminum and Iron Electrodes. *Ind. Eng. Chem. Res.* **2007**, *46*, 6189−6195.
(22) Farrell, J.; Wang, J.; O'Day, P.; Conklin, M. Electrochemical and Spectroscopic Study of Arsenate Removal from Water Using Zero-Valent Iron Media. *Environ. Sci. Technol.* **2001**, *35*, 2026−2032.
(23) Kanel, S. R.; Manning, B.; Charlet, L.; Choi, H. Removal of Arsenic(III) from Groundwater by Nanoscale Zero-Valent Iron. *Environ. Sci. Technol.* **2005**, *39*, 1291−1298.
(24) Moreno C, H. A.; Cocke, D. L.; Gomes, J. A. G.; Morkovsky, P.; Parga, J. R.; Peterson, E.; Garcia, C. Electrochemical Reactions for Electrocoagulation Using Iron Electrodes. *Ind. Eng. Chem. Res.* **2009**, *48*, 2275−2282.
(25) Van Genuchten, C. M.; Addy, S. E. A.; Peña, J.; Gadgil, A. J. Removing arsenic from synthetic groundwater with iron electrocoagulation: an Fe and As K-edge EXAFS study. *Environ. Sci. Technol.* **2012**, *46*, 986−994.
(26) Furukawa, Y.; Kim, J.; Watkins, J.; Wilkin, R. T. Formation of Ferrihydrite and Associated Iron Corrosion Products in Permeable Reactive Barriers of Zero-Valent Iron. *Environ. Sci. Technol.* **2002**, *36*, 5469−5475.
(27) Pascal, C.; Pascal, J. L.; Favier, F.; Elidrissi Moubtassim, M. L.; Payen, C. Electrochemical Synthesis for the Control of γ-Fe $_2O_3$ Nanoparticle Size. Morphology, Microstructure, and Magnetic Behavior. *Chem. Mater.* **1999**, *11*, 141−147.
(28) Misawa, T.; Hashimoto, K.; Shimodaira, S. Formation of $Fe(II)_1$-$Fe(III)_1$ intermediate green complex on oxidation of ferrous ion in neutral and slightly alkaline sulphate solutions. *J. Inorg. Nucl. Chem.* **1973**, *35*, 4167−4174.
(29) Géhin, A.; Ruby, C.; Abdelmoula, M.; Benali, O.; Ghanbaja, J.; Refait, P.; Génin, J.-M. R. Synthesis of Fe(II-III) hydroxysulphate green rust by coprecipitation. *Solid State Sci.* **2002**, *4*, 61−66.
(30) Amrose, S. E.; Bandaru, S. R. S.; Delaire, C.; van Genuchten, C. M.; Dutta, A.; Debsarkar, A.; Orr, C.; Das, A.; Roy, J.; Gadgil, A. Electro-chemical arsenic remediation: field trials in West Bengal. *Sci. Total Environ.* **2013**, in press.
(31) Phillips, D. H.; Van Nooten, T.; Bastiaens, L.; Russell, M. I.; Dickson, K.; Plant, S.; Ahad, J. M. E.; Newton, T.; Elliot, T.; Kalin, R. M. Ten year performance evaluation of a field-scale zero-valent iron permeable reactive barrier installed to remediate trichloroethene contaminated groundwater. *Environ. Sci. Technol.* **2010**, *44*, 3861−3869.
(32) Dubrawski, K. L.; Mohseni, M. In-situ identification of iron electrocoagulation speciation and application for natural organic matter (NOM) removal. *Water Res.* **2013**, *47*, 5371−5380.
(33) Amrose, S.; Gadgil, A.; Srinivasan, V.; Kowolik, K.; Muller, M.; Huang, J.; Kostecki, R. Arsenic removal from groundwater using iron electrocoagulation: effect of charge dosage rate. *J. Environ. Sci. Health, A: Tox. Hazard. Subst. Environ. Eng.* **2013**, *48*, 1019−1030.
(34) Bonin, P. M. L.; Odziemkowski, M. S.; Reardon, E. J.; Gillham, R. W. In Situ Identification of Carbonate-Containing Green Rust on Iron Electrodes in Solutions Simulating Groundwater. *J. Solution Chem.* **2000**, *29*, 1061−1074.
(35) Hansen, H. C. B. Composition, stabilization, and light absorption of Fe(II)Fe(III) hydroxy-carbonate (green rust). *Clay Miner.* **1989**, *24*, 663−669.
(36) Dubrawski, K. L.; Du, C.; Mohseni, M. General Potential-Current Model and Validation for Electrocoagulation. *Electrochim. Acta* **2014**, *129*, 187−195.
(37) Kaegi, R.; Voegelin, A.; Folini, D.; Hug, S. J. Effect of phosphate, silicate, and Ca on the morphology, structure and elemental composition of Fe(III)-precipitates formed in aerated Fe(II) and As(III) containing water. *Geochim. Cosmochim. Acta* **2010**, *74*, 5798−5816.
(38) Voegelin, A.; Kaegi, R.; Frommer, J.; Vantelon, D.; Hug, S. J. Effect of phosphate, silicate, and Ca on Fe(III)-precipitates formed in aerated Fe(II)- and As(III)-containing water studied by X-ray absorption spectroscopy. *Geochim. Cosmochim. Acta* **2010**, *74*, 164−186.
(39) Van Genuchten, C. M.; Peña, J.; Amrose, S. E.; Gadgil, A. J. Structure of Fe(III) precipitates generated by the electrolytic dissolution of Fe(0) in the presence of groundwater ions. *Geochim. Cosmochim. Acta* **2014**, *127*, 285−304.
(40) Regazzoni, A. E.; Urrutia, G. A.; Blesa, M. A.; Maroto, A. J. G. Some observations on the composition and morphology of synthetic magnetites obtained by different routes. *J. Inorg. Nucl. Chem.* **1981**, *43*, 1489−1493.
(41) Refait, P.; Bourdoiseau, J. A.; Jeannin, M.; Nguyen, D. D.; Romaine, A.; Sabot, R. Electrochemical formation of carbonated corrosion products on carbon steel in deaerated solutions. *Electrochim. Acta* **2012**, *79*, 210−217.
(42) Shipko, F. J.; Douglas, D. L. Stability of Ferrous Hydroxide Precipitates. *J. Phys. Chem.* **1956**, *60*, 1519−1523.
(43) Mechelhoff, M. *Electrochemical investigation of electrocoagulation reactors for water purification;* Imperial College: London, 2009.
(44) Dubrawski, K.; Du, C.; Mohseni, M. General Potential-Current Model and Validation for Electrocoagulation. *Electrochim. Acta* **2014**, *129*, 187−195.
(45) Murphy, O. J.; Bockris, J. O. M.; Pou, T. E.; Tongson, L. L.; Monkowski, M. D. Chloride ion penetration of passive films on iron. *J. Electrochem. Soc.* **1983**, *130*, 1792−1794.
(46) Lee, W.-J.; Pyun, S.-I. Effects of sulphate ion additives on the pitting corrosion of pure aluminium in 0.01 M NaCl solution. *Electrochim. Acta* **2000**, *45*, 1901−1910.
(47) Bourrié, G.; Trollard, F. Identification criteria for fougerite and nature of the interlayered anion. *19th World Congress Soil Sci. Soil Solutions for a Changing World*, 2010, Australian Society of Soil Science Incorporated: Warragul, Victoria, Australia.
(48) Refait, P.; Memet, J.-B.; Bon, C.; Sabot, R.; Genin, J.-M. R. Formation of the Fe(II)-Fe(III) hydroxysulphate green rust during marine corrosion of steel. *Corros. Sci.* **2003**, *45*, 13.
(49) Odziemkowski, M.; Flis, J.; Irish, D. E. Raman spectral and electrochemical studies of surface film formation on iron and its alloys

DOI: 10.1021/es505059d
Environ. Sci. Technol. 2015, 49, 2171−2179

with carbon in Na_2CO_3/$NaHCO_3$ solution with reference to stress corrosion cracking. *Electrochim. Acta* **1994**, *39*, 2225−2236.
(50) Ruby, C.; Abdelmoula, M.; Naille, S.; Renard, A.; Khare, V.; Ona-Nguema, G.; Morin, G.; Génin, J.-M. R. Oxidation modes and thermodynamics of FeII−III oxyhydroxycarbonate green rust: Dissolution−precipitation versus in situ deprotonation. *Geochim. Cosmochim. Acta* **2010**, *74*, 953−966.
(51) Stumm, W.; Morgan, J. J. *Aquatic Chemistry: An Introduction Emphasizing Chemical Equilibria in Natural Waters*; John Wiley & Sons Inc.: New York, 1970; p 583.
(52) Refait, P.; Reffass, M.; Landoulsi, J.; Sabot, R.; Jeannin, M. Role of phosphate species during the formation and transformation of the Fe(II−III) hydroxycarbonate green rust. *Colloids Surf., A: Physicochem. Eng. Asp.* **2007**, *299*, 29−37.
(53) Wang, Y.; Morin, G.; Ona-Nguema, G.; Juillot, F.; Calas, G.; Brown, G. E. Distinctive arsenic(V) trapping modes by magnetite nanoparticles induced by different sorption processes. *Environ. Sci. Technol.* **2011**, *45*, 7258−7266.
(54) Auffan, M.; Rose, J.; Proux, O.; Borschneck, D.; Masion, A.; Chaurand, P.; Hazemann, J.-L.; Chaneac, C.; Jolivet, J.-P.; Wiesner, M. R.; et al. Enhanced adsorption of arsenic onto maghemites nanoparticles: As(III) as a probe of the surface structure and heterogeneity. *Langmuir* **2008**, *24*, 3215−3222.
(55) Gui, J.; Devine, T. M. A SERS investigation of the passive films formed on iron in mildly alkaline solutions of carbonate/bicarbonate and nitrate. *Corros. Sci.* **1995**, *37*, 1177−1189.
(56) Dunnwald, J.; Dunnwald, J.; Otto, A. An investigation of phase transitions in rust layers using raman spectroscopy. *Corros. Sci.* **1989**, *29*, 1167−1176.

DOI: 10.1021/es505059d
Environ. Sci. Technol. 2015, 49, 2171−2179